UNIVERSITY OF LEEDS

This is a repository copy of *Thermal Characteristics and Kinetic Analysis of Woody Biomass Pyrolysis in the Presence of Bifunctional Alkali Metal Ceramics*.

White Rose Research Online URL for this paper:
http://eprints.whiterose.ac.uk/142265/

Version: Accepted Version

Article:
Vuppaladadiyam, AK, Memon, MZ, Ji, G et al. (4 more authors) (2019) Thermal Characteristics and Kinetic Analysis of Woody Biomass Pyrolysis in the Presence of Bifunctional Alkali Metal Ceramics. ACS Sustainable Chemistry and Engineering, 7 (1). pp. 238-248. ISSN 2168-0485

https://doi.org/10.1021/acssuschemeng.8b02967

Copyright © 2018 American Chemical Society. This document is the unedited Author's version of a Submitted Work that was subsequently accepted for publication in ACS Sustainable Chemistry and Engineering, To access the final edited and published work see http://doi.org/10.1021/acssuschemeng.8b02967.

Reuse
Items deposited in White Rose Research Online are protected by copyright, with all rights reserved unless indicated otherwise. They may be downloaded and/or printed for private study, or other acts as permitted by national copyright laws. The publisher or other rights holders may allow further reproduction and re-use of the full text version. This is indicated by the licence information on the White Rose Research Online record for the item.

Takedown
If you consider content in White Rose Research Online to be in breach of UK law, please notify us by emailing eprints@whiterose.ac.uk including the URL of the record and the reason for the withdrawal request.

White Rose university consortium
Universities of Leeds, Sheffield & York

eprints@whiterose.ac.uk
https://eprints.whiterose.ac.uk/

published ACS Sustainable Chem. Eng. 2019, 7, 238−248

Thermal characteristics and kinetic analysis of woody biomass pyrolysis in presence of bifunctional alkali metal ceramics

Arun K. Vuppaladadiyam[†], Muhammad Zaki Memon[†], Guozhao Ji[†], Abdul Raheem[†], Valerie Dupont[‡] and Ming Zhao[†⁑,]*

[†] School of Environment, Tsinghua University, Beijing 100084, China.

[‡]School of Chemical and Process Engineering, The University of Leeds, LS2 9JT, UK

[⁑], Key Laboratory for Solid Waste Management and Environment Safety, Ministry of Education, Beijing, 100084, China

***Keywords*:** Woody biomass, alkali metal ceramics, in-situ CO_2 capture, kinetic analysis, *iso*-conversional methods.

ABSTRACT: Effects of alkali ceramics, Na_2ZrO_3 (NZ) and Li_4SiO_4 (LS), were quantified in the catalytic pyrolysis of sawdust, using thermogravimetric analysis and kinetic modeling. Results indicated that the alkali ceramics were able to initiate thermal decomposition at lower

temperatures and enhanced H_2 yield. The mean activation energies estimated by Kissinger-Akahira-Sunose (KAS) and Flynn-Wall-Ozawa (FWO) methods were within the range of 164-166, 114-116, 112-117 kJ mol^{-1} for sawdust (SD), sawdust mixed with Li_4SiO_4 (SD-LS) and sawdust mixed with Na_2ZrO_3 (SD-NZ), respectively. The theoretical and experimental master plots constructed for SD closely match with theoretical master plot corresponding to three-dimensional diffusion (Ginstling-Brounshtein equation) (D4) reaction model. The SD-LS and SD-NZ samples followed first order (F1) reaction model at lower conversions and shifted from F1 to three-dimensional diffusion (D4) reaction model at higher conversions.

Graphical abstract

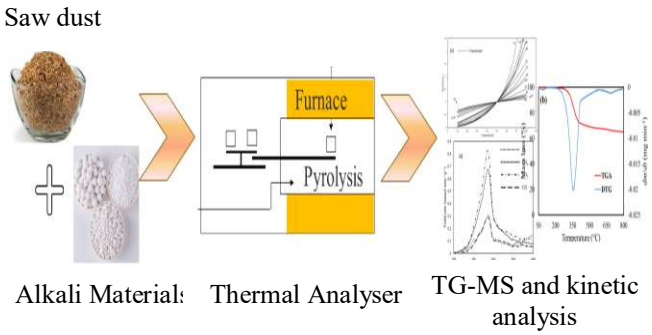

SYNOPSIS. Knowledge of thermal and kinetic behavior of biomass is essential is developing sustainable energy conversion processes.

■ Introduction

Increase in energy demand, depleting fossil fuel reserves and climate change have spurred energy experts and researchers to search for clean alternative energy resources. In comparison to fossil fuels, certain types of biomass, such as agricultural and forest wastes, can be considered as sustainable and eco-friendly energy resources in terms of reduction in pollution and global warming.[1] Lignocellulosic biomass, in particular, is considered as an ideal feedstock for

thermochemical processes to produce energy-related products.[2] It is estimated that China produces around 728–750 and 200–220 Mt yr^{-1} of agricultural residues and forest biomass, respectively.[3]

Pyrolysis is one of the most widely applied method used to convert biomass into high-energy content fuels, which can later be used for internal combustion engines and gas turbines after an intermediate process.[4] When compared to gasification and combustion, pyrolysis possesses the following advantages: (i) it does not require high temperatures, as liquid production can be maximized with low vapour residence time (up to 5 s) and vapour temperature less than 400 °C (ii) anaerobic conditions, which produce biochar that can be used as soil additive and (iii) generation of high quality of oil,[2] which contain 200 types of organic compounds that can serve as a source of pure chemicals such as organic acids, aldehydes, etc. However, several different types of oxygenated compounds are generated during biomass pyrolysis because of complex structure of biomass and various reaction pathways. These oxygenated compounds make bio-oil incompatible with petroleum based infrastructure. Catalytic pyrolysis has been investigated as a method to optimize the distribution of desired products by selectively enhancing a specific reaction.[5] Alkali metals, such as sodium (Na) and potassium (K), are widely reported to show notable catalytic effect on biomass pyrolysis.[6, 7] The addition of potassium salts improved the product distribution and promoted the fragmentation and depolymerization of biomass components during pyrolysis.[6, 8]

Thermal decomposition is a complicated process and involves hundreds of consecutive and/or parallel reactions. The biomass decomposition usually ensues in three regions representing water evaporation, active pyrolysis and passive pyrolysis.[9] The decompositions of cellulose and hemicellulose occur during the active pyrolysis in temperature range of 523 to 653 K and 473 to

653 K respectively. Lignin decomposition takes place in both active and passive pyrolysis in temperature range 453 to 1173 K.[10] It is to be noted that the solid residue left at the end of the pyrolysis (char and mineral matter) largely depends on the source biomass. Moreover, the process of thermal decomposition is influenced by operational parameters such as temperature, heating rate, size and shape of biomass etc.

The *iso*-conversional methods are highly recommended by International Confederation for Thermal Analysis and Calorimetry (ICTAC) to evaluate the 'kinetic triplet' that includes apparent activation energy, pre-exponential factor and reaction mechanism.[11] The list of differential expressions $f(\alpha)$ and integral expressions $g(\alpha)$ of mechanism functions tested in the present study are presented in **Table 1**. It should be noted that most of models specified in Table 1 are relevant to solid-state reactions. It is always important to confirm if a solid substance would react in solid state upon heating. It is to be understood that once heating has begun, before the reaction starts any solid substance may melt and the reaction may take place in liquid phase. It is advisable to use a reaction model that is appropriate to the process being studied. However, all the reaction models that are available can be reduced into three major types: accelerating (e.g., power-law models), decelerating (e.g., reaction-order and diffusion models), and sigmoidal (e.g., Avrami-Erofeev models) types.[12] The present study investigates the thermal decomposition characteristics of sawdust, with and without alkali ceramic bifunctional materials, at multiple heating rates. The studied samples include sawdust (SD), sawdust mixed with lithium silicate (SD-LS) and sawdust mixed with sodium zirconate (SD-NZ). The evolution trends of various pyrolysis gases were analyzed and reported. The kinetic parameters, apparent activation energy was identified by using Kissinger-Akhira-Sunose (KAS)[13] and Flynn-Wall-Ozawa (FWO)[14, 15]

methods. The pyrolysis reaction mechanism function $f(\alpha)$ was identified by using generalized master plots method[16].

Table 1. Most common reaction mechanisms in solid stare reactions.[17, 18]

Mechanism – Solid state process	Differential form $f(\alpha)$	Integral form $g(\alpha)$
A_2 – Nucleation and growth (Avrami Eqn. 1)	$2(1-\alpha)[-\ln(1-\alpha)]^{1/2}$	$[-\ln(1-\alpha)]^{1/2}$
A_3 – Nucleation and growth (Avrami Eqn. 2)	$3(1-\alpha)[-\ln(1-\alpha)]^{3/2}$	$[-\ln(1-\alpha)]^{1/3}$
A_4 – Nucleation and growth (Avrami Eqn. 3)	$4(1-\alpha)[-\ln(1-\alpha)]^{3/4}$	$[-\ln(1-\alpha)]^{1/4}$
R_2 – Phase boundary controlled reaction (contracting area)	$2(1-\alpha)^{1/2}$	$[1-(1-\alpha)]^{1/2}$
R_3 – Phase boundary controlled reaction (contracting volume)	$3(1-\alpha)^{2/3}$	$[1-(1-\alpha)]^{1/3}$
D_1 – One-dimensional diffusion	$(1/2)\alpha$	α^2
D_2 – Two-dimensional diffusion (Valensi equation)	$[-\ln(1-\alpha)]^{-1}$	$(1-\alpha)\ln(1-\alpha)+\alpha$
D_3 – Three-dimensional diffusion (Jander equation)	$(3/2)[1-(1-\alpha)^{1/3}]^{-1}(1-\alpha)^{2/3}$	$[1-(1-\alpha)^{1/3}]^2$
D_4 – Three-dimensional diffusion (Ginstling-Brounshtein equation)	$(3/2)[1-(1-\alpha)^{1/3}]^{-1}$	$[1-(2/3)\alpha)]-(1-\alpha)^{2/3}$
F_1 – Random nucleation with one nucleus on the individual particle	$1-\alpha$	$-\ln(1-\alpha)$
F_2 – Random nucleation with two nuclei on the individual particle	$(1-\alpha)^2$	$1/(1-\alpha)$
F_3 – Random nucleation with three nuclei on the individual particle	$(1/2)(1-\alpha)^3$	$1/(1-\alpha)^2$
P_1– Mampel power law ($n = 1/2$)	$2\alpha^{1/2}$	$\alpha^{1/2}$
P_2 – Mampel power law ($n = 1/3$)	$3\alpha^{2/3}$	$\alpha^{1/3}$
P_3 – Mampel power law ($n = 1/4$)	$4\alpha^{3/4}$	$\alpha^{1/4}$

■ EXPERIMENTAL SECTION

Biomass Characterization. Sawdust (SD) was selected as waste biomass for pyrolysis experiments. The biomass samples were processed in a grinder and then were sieved to a diameter less than 0.2 μm. Ultimate and proximate analyses were performed to characterize the biomass. To detect carbon, hydrogen, oxygen, and nitrogen fractions in the biomass, a EuroEA3000 Elemental Analyser was used, while, 5E-AS3200B Automatic Coulomb Sulfur Analyzer identified the sulfur fraction. The values obtained from proximate, ultimate and structural components analysis of sawdust are presented in **Table 2.**

Table 2. Characterization of sawdust samples.

Proximate Analysis (wt. %)		Ultimate analysis (dry wt. %)		Structural component analysis (wt. %)	
Moisture content	9.85	C	45.93	Lignin	21.5
Volatile matter	72.92	H	6.26	Cellulose	50.03
Ash	0.27	O	44.54	Hemicellulose	24.8
Fixed Carbon	16.97	N	0.12	Others	3.4
		S	0.04		

The bifunctional materials Na_2ZrO_3 (NZ) and Li_4SiO_4 (LS) were synthesized according to methods previously investigated by our group and a detailed explanation of the synthesis methods and characterization can be found in the literature.[19, 20]

TG-DTG-MS Analysis. The thermogravimetric (TG) and derivative thermogravimetric (DTG) analyses were performed in a thermal analyzer (Q600). The experiments were divided in two sets. The first set of experiments was run at a constant heating rate of 35 °C min^{-1} for the selected waste biomass samples and biomass samples mixed with the two alkali ceramics. Each sample weighing 3 mg was heated from ambient temperature to 600 °C. The second set of experiments was run at multiple heating rates, 40 and 45 °C min^{-1}, from ambient temperature to

600 °C for both plain and blended samples. The biomass and bifunctional materials were mechanically mixed at 1:1 ratio (w/w) for the experiments run at three heating rates. Argon (Ar) gas, with a flow rate of 500 mL min^{-1}, was used to maintain the inert gas atmosphere within the system. All the experiments were conducted in triplicate and the results reported were the average of the obtained data.

The mass spectrometer (MS) ionizes the gas molecules collected by heated capillary and differentiates the resulting positive ions on the basis of their mass to charge ratio (*m/z*). The ions set to be scanned and their corresponding evolved gas species are given in **Table 3**.

Table 3. Key ion fragments and representative evolved gas species.

m/z	Ion fragments	Representative Species
2	H_2^+	Hydrogen
15	CH_3^+	Methane
28	CO^+	Carbon monoxide
40	Ar^+	Argon
44	CO_2^+	Carbon dioxide

The raw signals received obtained from MS were normalized relative to constant Ar purge and weight of biomass (Eqn. 1)

Normalized signal for key molecule fragments 'i' = $(IC_i*500)/(IC_{Ar}*wt._{sample})$ (1)

In the Eqn. (1), IC_i stands for molecular m/z signals for molecular ion fragments 'i' (arbitrary unit), IC_{Ar} is the m/z signals for Ar, and $wt._{sample}$ is the weight of sample (g). The normalized ion current signals from MS were expressed as instant volume concentrations of gas products contained in carrier gas (Ar, 500 mL min^{-1}, and 25 °C, 1 atm). The total gas product (mL mg^{-1}) was obtained by integrating the normalized curves obtained from the plot generation rate (mL

min^{-1} g^{-1}) vs. reaction temperature. The temperature region in which maximum gas yield occurred was chosen for integration and it should be noted that all the volume related units are presented at normal conditions (25 ^{o}C, 1 atm). The gas yields obtained in mL min^{-1} g^{-1} where then converted into mmol g^{-1} and then where reported.

Kinetic Analyses. Pyrolysis of biomass varies because of variations in the chemical composition of compounds in the biomass material. However, the overall path of biomass pyrolysis can be defined as; $\text{Biomass} \rightarrow \text{Char} + \text{Volatiles} + \text{Gases}$. According to the Arrhenius equation, the rate constant k(T) is expressed as follows:

$$k(T) = Ae^{(\frac{-E_\alpha}{RT})} \qquad (2)$$

where A (s^{-1}) is the pre-exponential (or "frequency") factor, E_α (J mole^{-1}) is the activation energy of the reaction, R is the universal gas constant (8.314 J mol^{-1} K^{-1}), and T (°K) is the absolute temperature. When applied to an overall reaction mechanism, the activation energy for the ensemble of reactions is termed "apparent".

According to Mishra et al. (2014), the kinetics of heterogeneous solid-state thermal degradation can be defined as [21]:

$$\frac{d\alpha}{dt} = k(T)\, f(\alpha) = Ae^{(\frac{-E_\alpha}{RT})}\, f(\alpha) \qquad (3)$$

where α is the fractional conversion (or conversion degree) of the main reactant at time t, f (α) represents a reaction function depending on the conversion rate in relation to reaction model at the conversion degree α and t stands for time.

Taking the logarithm of Eq. (3) and lumping $A(\alpha)f(\alpha)$ to give Friedman's method,[22]

$$\ln\left(\frac{d\alpha}{dt}\right) = \ln\left[A(\alpha)\, f(\alpha)\right] - \frac{E_a(\alpha)}{RT} \qquad (4)$$

The conversion degree α reflects the thermal decomposition and is defined as

$$\alpha = \frac{m_0 - m_t}{m_0 - m_\infty} \quad (5)$$

where m_0, m_t, m_∞ are initial, instantaneous and final masses during thermal degradation, respectively.

Taking into consideration that the temperature is a function of time and is increasing with a constant heating rate β, then β can be expressed as

$$\beta = \frac{dT}{dt} = \frac{dT}{d\alpha} \times \frac{d\alpha}{dt} \quad (6)$$

Rearranging Eqns. (3) and (6)

$$\frac{d\alpha}{dT} = \frac{A}{\beta} e^{(\frac{-E_\alpha}{RT})} f(\alpha) \quad (7)$$

The integrated form of f (α) is generally stated as:

$$g(\alpha) = \int_0^\alpha \frac{d\alpha}{f(\alpha)} = \frac{A}{\beta} \int_{T_0}^{T} e^{(\frac{-E_a}{RT})} dT \quad (8)$$

The above integral equation has no exact solution. Thus, Eqn. (8) can be solved by approximations or numerical methods. Considering the good adaptability and validity for their model-free approaches, the iso-conversional methods are known to provide a feasible approach to estimate the activation energy and pre-exponential factor. Thus, three iso-conversional methods: Kissinger-Akahira-Sunose (KAS), Flynn-Wall-Ozawa (FWO) and Friedman method (FM), are used for the determination of kinetic parameters.

The FWO method can be expressed as follows:

$$\ln(\beta) = \ln[\frac{AE_\alpha}{R\, g(\alpha)}] - 5.331 - 1.0516 \frac{E_\alpha}{RT} \quad (9)$$

The KAS method can be expressed as follows:

$$\ln(\frac{\beta}{T^2}) = \ln[\frac{AR}{E_\alpha\ g(\alpha)}] - \frac{E_\alpha}{RT} \qquad (10)$$

At constant conversion rate α, the plots $\ln(\beta/T^2)$ vs. 1/T (KAS method), ln (β) vs. 1/T (FWO method) and $\ln(d\alpha/dt)$ vs. 1/T (Friedman method) obtained from TG plots ($100\times(1-m/m_0)$ vs. T) at several heating rates result in straight lines, for which the slopes and intercepts help determine the apparent activation energy and pre-exponential factor. In order to identify the most probable mechanism function g (α), integral master plots methods was adopted. Although, master plots are theoretical curves that depend on kinetic model, they are independent of kinetic parameters such as activation energy and pre-exponential factor. Theoretical master plots, listed in Table 1, were considered as a reference for determining the best fit kinetic model for a solid-state reaction. Experimental master plots were constructed and then compared to theoretical master plots. The most probable kinetic model can be determined by the integral master-plot method proposed by Gotor[23]. The concept underlying the generalized master plots method is the generalized time (θ), at infinite temperature, required to achieve a given conversion (α)[24, 25] and obeys the equation below

$$\theta = \int_0^t e^{\left(\frac{-E_\alpha}{RT}\right)} dt \qquad (11)$$

Using the integral kinetic equation at infinite temperature in integral form, Eqn. (8), by considering $\alpha = 0.5$ as a reference point we can obtain the following equation.

$$\frac{g(\alpha)}{g(\alpha)_{0.5}} = \frac{\theta}{\theta_{0.5}} \qquad (12)$$

where $\theta_{0.5}$ is the generalized time at $\alpha = 0.5$.

Under non-isothermal conditions with linear heating rate, β, from Eqn. (11), the value of θ, at any given α can be obtained from the following equation.

$$\theta = \frac{1}{\beta}\int_0^T e^{\left(\frac{-E_\alpha}{RT}\right)} dT = \frac{E}{\beta R}\int_x^\infty \frac{e^{(-x)}}{x^2} dx = \frac{E}{\beta R} P(x) \qquad (13)$$

where x = E/RT. The function P(x) in Eqn. (13) does not have analytical solution and can be expressed by an approximation. In this study, secondary rational approximation of Senum and Yang[26] is used. Therefore, for a linear heating rate $\theta/\theta_{0.5}$ values can be obtained from the following equation.

$$\frac{\theta}{\theta_{0.5}} = \frac{P(x)}{P(x_{0.5})} \qquad (14)$$

From Eqns. (12) and (14), considering α = 0.5 as a reference point we can relate the appropriate kinetic model to reduced generalized rate of reaction as given below

$$\frac{g(\alpha)}{g(\alpha)_{0.5}} = \frac{\theta}{\theta_{0.5}} = \frac{P(x)}{P(x_{0.5})} \qquad (15)$$

Therefore, by plotting the generalized reaction rate from (15), and the fraction $g(\alpha)/g(\alpha_{0.5})$ listed in Table 1 against conversion (α), an appropriate kinetic model can be inferred on comparison.

The pre-exponential factor (A) and other thermodynamic parameters such as, enthalpy (ΔH), free Gibbs energy (ΔG), and changes in entropy (ΔS) were expressed using Eqs. (16) to (19)[27, 28]:

$$A = \beta \cdot E_\alpha \cdot e^{\left(\frac{E_\alpha}{RT_m}\right)} \Big/ \left(R \cdot T_m^{\,2}\right) \qquad (16)$$

$$\Delta H = E_\alpha - RT \qquad (17)$$

$$\Delta G = E_\alpha + RT_m \cdot \ln\left[\frac{k_B T_m}{h A}\right] \qquad (18)$$

$$\Delta S = \frac{\Delta H - \Delta G}{T_m} \qquad (19)$$

where, k_B is the Boltzmann constant (1.381×10^{-23} J K^{-1}); T_m is the DTG peak temperature; h is the Plank constant (6.626×10^{-34} J s).

■ RESULTS AND DISCUSSION

Pyrolysis Behavior of Sawdust under Catalytic and Non-catalytic Conditions. The TG (mass % loss vs. T) and DTG (dm/dt vs. T) curves of the pyrolysis process for samples, which include SD, SD-NZ and SD-LS at heating rate 35 °C min^{-1} are presented in **Fig. 1**. Pyrolysis decomposes the organic components of a material into different vapor phases and gas compounds leaving char as residue. The main pyrolysis of the plain sample, SD, took place between 200 and 500 °C and is in good agreement with other studies, with feedstock of similar category, reported in the literature.[29-31] During pyrolysis, the mass loss in samples is because of vapor and gas evolution. The pyrolysis of samples, with and without alkali materials, can be divided in to three stages. The first stage corresponds to dehydration (< 200 °C), where moisture gets extracted from the samples. A small quantity of hemicellulose, as it acts as a link between cellulose and lignin, starts decomposing in this stage.[29] The second stage of the pyrolysis is considered as the main decomposition stage and a dramatic change can be noticed in the DTG curve during the second stage of decomposition. It can be noticed from Fig. 1 that a little devolatilization occurred at around 250 °C and proceeded rapidly with increasing temperature. The peak temperature for SD, where maximum mass loss occurred, was noticed at 388 °C, after which, the mass loss decreased gradually.

The impact of catalytic activity of alkali materials was evident in the mass loss pattern during pyrolysis. The maxima of mass loss for samples SD-NZ and SD-LS were lower than those registered for plain sample. This suggests the possibility of alkali metals (Li and Na) initiating the pyrolysis process at lower temperatures. The peak temperatures for SD-NZ and SD-LS were

359 and 361 °C respectively. Na_2ZrO_3 and Li_4SiO_4 have been shown in previous studies to exhibit catalytic activity in devolatilization. The results match the previous works with cellulose and Na_2ZrO_3, where the catalyst was able to lower the activation energy.[7] Further, the presence of third peak of mass loss was noticed at around 550 °C for all the samples and the reason can be attributed to a continuous period of catalytic breakdown of lignin.

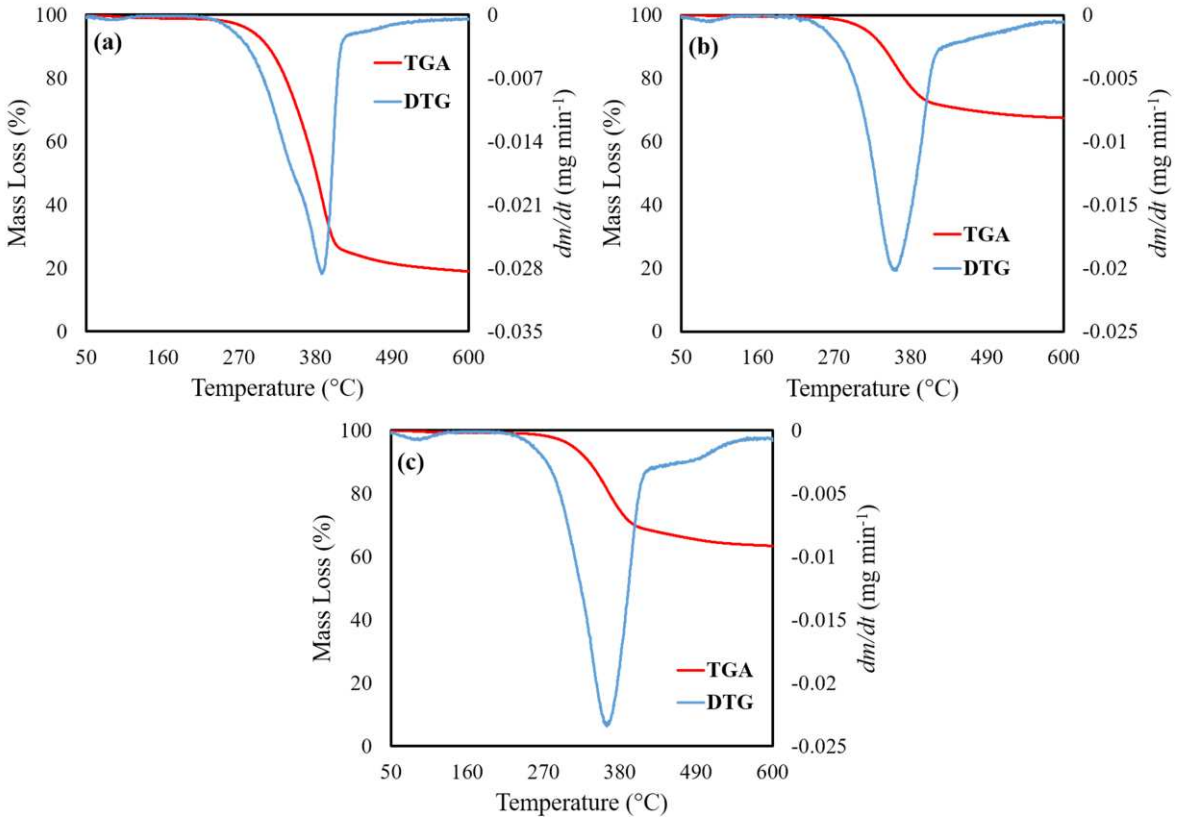

Figure 1. TG and DTG curves of plain and alkali metal mixed samples (a) SD and (b) SD-LS and (c) SD- NZ at heating rate 35 °C min^{-1}.

Analysis of Evolved Gas Species. Gas evolution from pyrolysis of samples SD, SD-LS and SD-NZ are shown in **Fig. 2a, 2b** and **2c** respectively**.** From the samples, syngas primarily evolved during the pyrolysis and, at temperatures above 500 °C a second peak of H_2 generation was observed. The emerging H_2 peak over 500 °C could be from multiple tar cracking and tar reforming reactions. CO and CO_2 were dominant species released during primary pyrolysis of

SD, and a small peak of CH_4 was also observed. The presence of alkali metals resulted in a dramatic effect on the release of H_2 after the primary pyrolysis phase. CH_4 and CO yield trends from SD-NZ and SD-LS samples are similar to SD samples, but H_2 and CO_2 trends appear to be suppressed in the presence of alkali metals.

The second H_2 peak for SD-NZ and SD-LS is due to the participation of Na_2ZrO_3 and Li_4SiO_4 in sorption enhanced reforming (SER) reactions as CO_2 sorbents. SER reactions depend on CO_2 removal to overcome thermodynamic limitations set on high-temperature endothermic steam reforming (SR) reactions, shown here with CH_4 as the feed in (Eqn. 20) and low-temperature exothermic water-gas shift (WGS) reaction (Eqn. 21).

$$CH_4 + H_2O \leftrightarrows 3H_2 + CO \qquad (20)$$

$$CO + H_2O \leftrightarrows H_2 + CO_2 \qquad (21)$$

Na_2ZrO_3, a more active CO_2 sorbent, captured CO_2 earlier, which resulted in H_2 peak from SD-NZ samples at temperatures around 450 °C, while Li_4SiO_4 participated in SESR at around 500 °C. The results are enhanced H_2 production. A similar results has been reported by Memon, et al.[7], where Na_2ZrO_3 enhanced H_2 production in similar manner during cellulose pyrolysis.

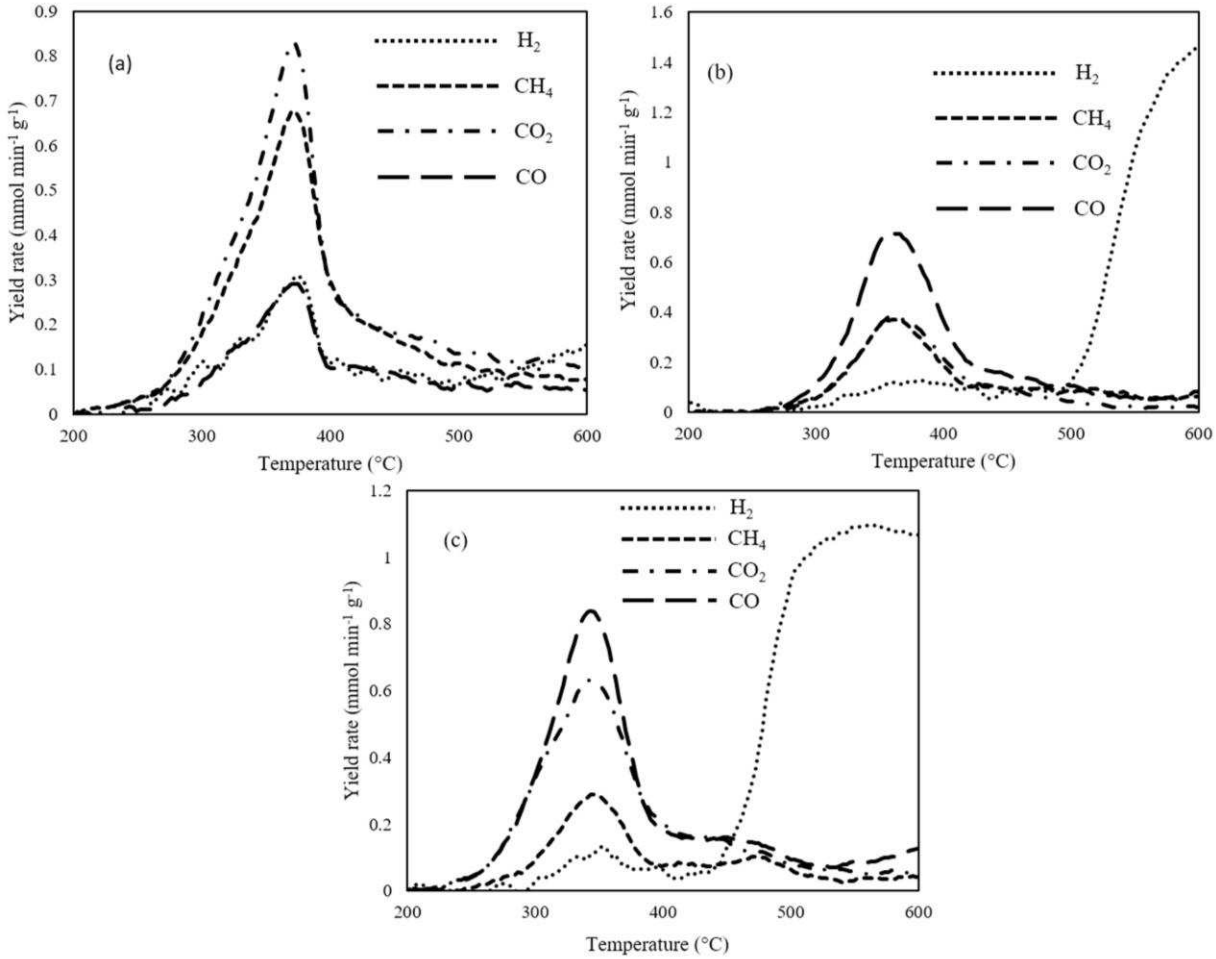

Fig. 2. Gas formation rates (H_2, CH_4, CO, CO_2) of (a) SD, (b) SD-LS and (c) SD- NZ

Kinetic Analysis. Thermogravimetric data was used to characterize the selected biomass samples as well as to study the reaction kinetics that result from thermal degradation. Chemical kinetics together with description of transport phenomena can be considered as useful information for the design and optimization of thermochemical systems.[32, 33] The linear correlations of pyrolysis for SD, SD-LS and SD-NZ were calculated by iso-conversional methods KAS and FWO at 35, 40 and 45 °C min^{-1} and are presented in **Fig. 3**. According to Eqns. (7) and (8) the apparent activation energies were calculated within a selected range of conversion 0.1 – 0.8 with a step of 0.1 and are listed in **Table 4**.

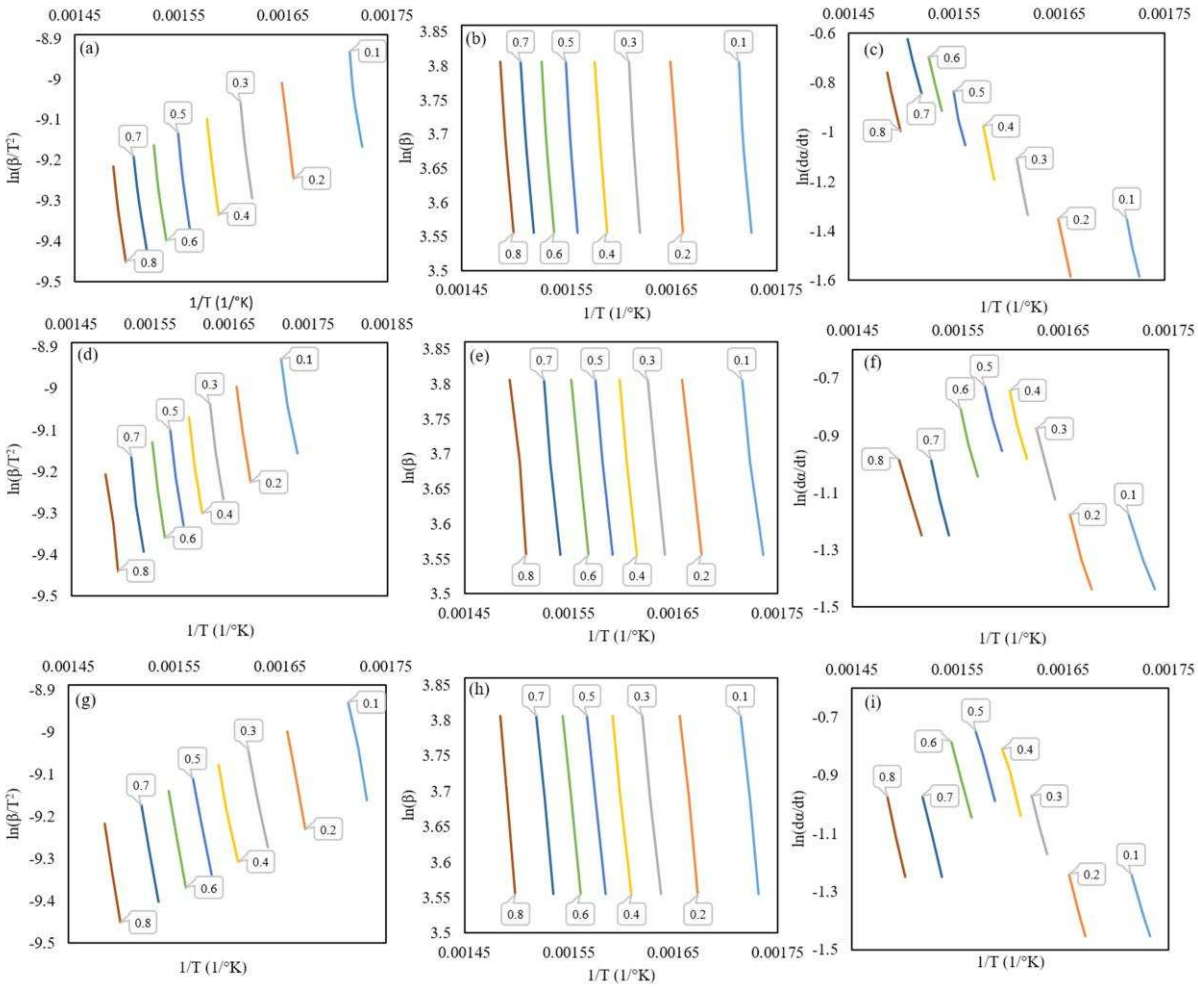

Fig. 3. Linear correlation of pyrolysis at 35, 40, 45 °C min^{-1} by (a) KAS (b) FWO (c) FM for SD, (d) KAS, (e) FWO (f) FM for SD-LS and (g) KAS, (h) FWO (i) FM for SD-NZ respectively.

Activation energy can be defined as the minimum energy necessary to initiate a reaction, which means that for a given pre-exponential factor, the higher the activation energy, the slower the reaction.[34] From the results shown in Table 4 it should be noted that the apparent activation energy (E_α) is highly dependent on the conversion, indicating the complexity of the biomass pyrolysis with many reactions occurring simultaneously at the same stage.[35] It can be noticed, from Table 4, that the E_α calculated from KAS and FWO methods remained stable with the conversion progressing in the range 0.2-0.5 for SD and a similar behavior was noticed for

samples mixed with alkali materials. It can also be noted that the E_α value is low at low conversion (α =0.1) when compared to the other stages of conversion, could possibly be influenced by the higher reaction rate. The rapid increase in the activation energy for SD samples from α = 0.2 indicate the initiation of main component pyrolysis.[36] During the estimation of E_α for a chemical reaction involving the physical transformation of biomass, it should be noted that the value of E_α correlates to the chemical stability of the compound. Therefore, to ensure the decomposition of stable compounds, it is necessary to supply more energy.

Table 4. Results of apparent activation energy (E_α) (kJ mol^{-1}) with KAS, FWO and Friedman methods

Method/ Material	Conversion (α)/ Parameters/	KAS		FWO		Friedman Method	
		E_α	R^2	E_α	R^2	E_α	R^2
SD	0.1	155.1	0.972	156.7	0.975	158.2	0.994
	0.2	171.5	0.999	172.6	1.000	170.0	1.000
	0.3	179.5	0.992	180.5	0.992	175.3	0.999
	0.4	170.9	0.998	172.5	0.998	168.1	1.000
	0.5	170.7	0.992	172.5	0.993	166.2	0.987
	0.6	159.7	0.987	162.2	0.989	156.0	0.998
	0.7	149.4	0.993	152.5	0.993	149.9	0.998
	0.8	155.6	0.993	158.5	0.994	155.7	0.998
	Average	164.0		166.0		162.4	
SD-LS	0.1	90.3	0.984	95.1	0.989	89.4	0.990
	0.2	104.2	0.999	108.6	1.000	103.2	0.993
	0.3	114.2	0.997	118.4	0.999	115.9	0.999
	0.4	114.1	0.987	119.1	0.993	118.2	0.986

	0.5	113.8	0.996	118.4	0.999	112.7	0.995
	0.6	117.1	0.996	121.7	1.000	120.0	0.996
	0.7	122.9	0.980	127.7	0.990	126.5	0.997
	0.8	123.3	0.982	125.4	0.997	123.3	1.000
	Average	112.6		116.8		113.7	
SD-NZ	0.1	109.3	0.993	113.1	0.994	110.8	0.998
	0.2	110.6	0.998	114.6	0.998	114.3	1.000
	0.3	105.0	0.997	109.5	0.997	111.7	1.000
	0.4	103.8	0.996	108.6	0.997	109.6	0.993
	0.5	106.2	1.000	111.0	1.000	113.9	0.999
	0.6	114.0	1.000	122.0	1.000	116.5	1.000
	0.7	115.9	1.000	120.4	0.998	124.4	0.999
	0.8	135.3	1.000	139.2	1.000	132.7	0.997
	Average	112.5		117.3		116.7	

It can be witnessed from the results that the E_α value for all the samples is found to decrease at higher conversions. This may be attributed to the fact that during the decomposition of stable compounds at high temperature, less stable compounds that are easier to decompose are formed resulting in the lowering the heat supply. Additionally, at higher temperatures, easily decomposable molecules formed art higher temperatures resulting in the decrease in activation energy at higher conversions.[33] The second stage of pyrolysis (major mass loss stage in the temperature range 200-600 °C) was considered for kinetic analysis, as it should be noted that the thermal degradation of major components of biomass, which include cellulose, hemicellulose and lignin, happens in the range of 200-600 °C.[37] According to Burhenne et al., higher values of activation energy are needed for the decomposition of biomass with high lignin content.[10] The E_α values varied from 149.4 to 179.5 kJ mole^{-1} for SD, whereas for samples mixed with alkali

materials, E_α were found to be low. The values varied from 90.3 to 136.2 kJ mole^{-1} and 103.8 to 135.3 kJ mole^{-1} for SD-LS and SD-NZ samples respectively. The reaction with higher E_α value needs longer retention time or elevated temperatures, which allows the reaction to gain sufficient energy. Thus the value of apparent activation energy could be used to differentiate the stages of reaction during thermal decomposition.[30] Furthermore, the average E_α values for all the samples considered in this study were lower than the average E_α values reported for rice husk (221–229 kJ mol^{-1}), elephant grass (218–227 kJ mol^{-1}),[38] cellulose (191 kJ mol^{-1}),[16] algae (154 -261 kJ mol^{-1})[39] and camel grass (168 -169 kJ mol^{-1})[40]. This indicates the suitability of SD for co-firing with other types of biomass.

The generalized master plots do not depend on heating rates used during experiments and strictly depend on the kinetic model used to fit the reaction. Therefore, in principle, the master plots generated experimentally under different heating rates should take similar shapes. The right hand side of Eqn. (13) vs. conversion, α, were used to construct master plots for every experimental curves by using the activation energy obtained from iso-conversional methods previously. Similarly, the theoretical master plots corresponding to different kinetic models mentioned in Table 1 are built by constructing the left hand side of Eqn. (13) vs. conversion, α. **Fig. 4** shows the comparison between theoretical and experimental master plots for SD (Fig. 4a), SD-LS (Fig. 4b) and SD-NZ (Fig. 4c). The integral master plots constructed for SD closely match with theoretical master plot corresponding to three-dimensional diffusion (Ginstling-Brounshtein equation) (D4) reaction model. For SD-LS and SD-NZ, the experimental master-plots were closely in accordance with random nucleation with one nucleus on the individual particle (F1) reaction model in the conversion range 0.1 – 0.6. At higher conversion rates, the reaction model shifted from F1 to three-dimensional diffusion (Ginstling-Brounshtein equation)

(D4) reaction model. It can be inferred that the synergistic effect of alkali metals on the biomass has similar influence on the degradation mechanisms. The degradation mechanism of SD-LS and SD-NZ were similar to each other and differed significantly from that of the plain sample SD. The little divergence of experimental master plot curves at few conversions, for all the samples considered in the study, could be attributed to the deviations of ideal conditions assumed in kinetic models with real conditions.

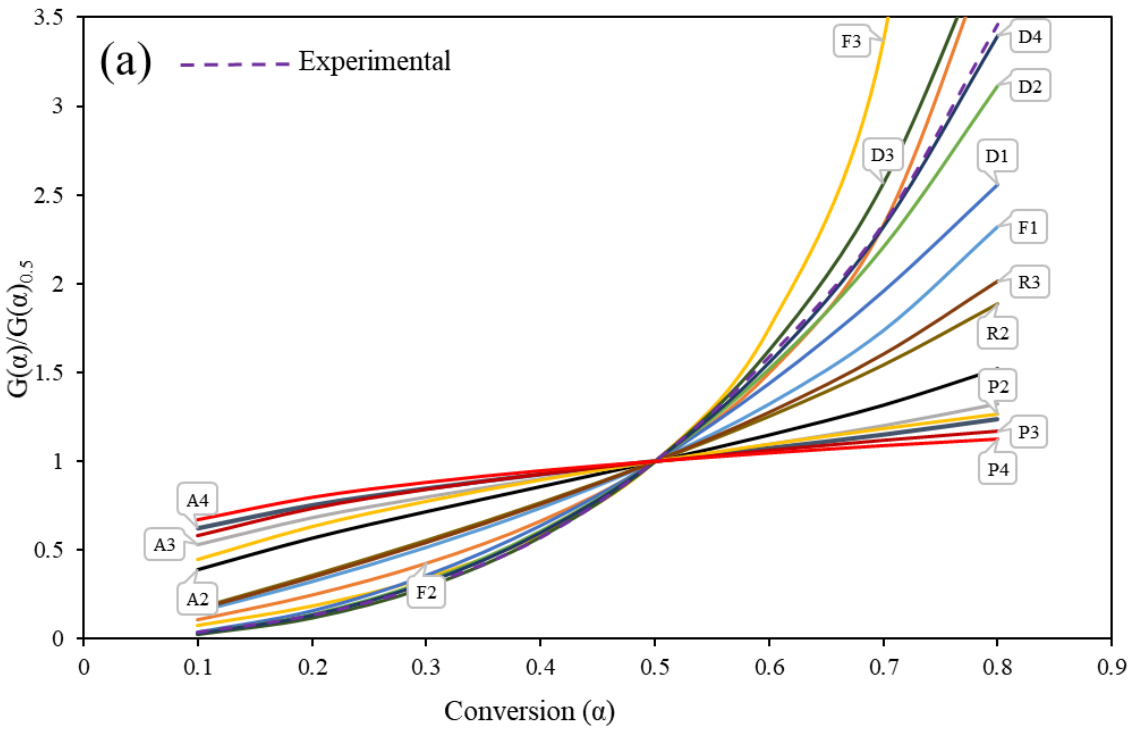

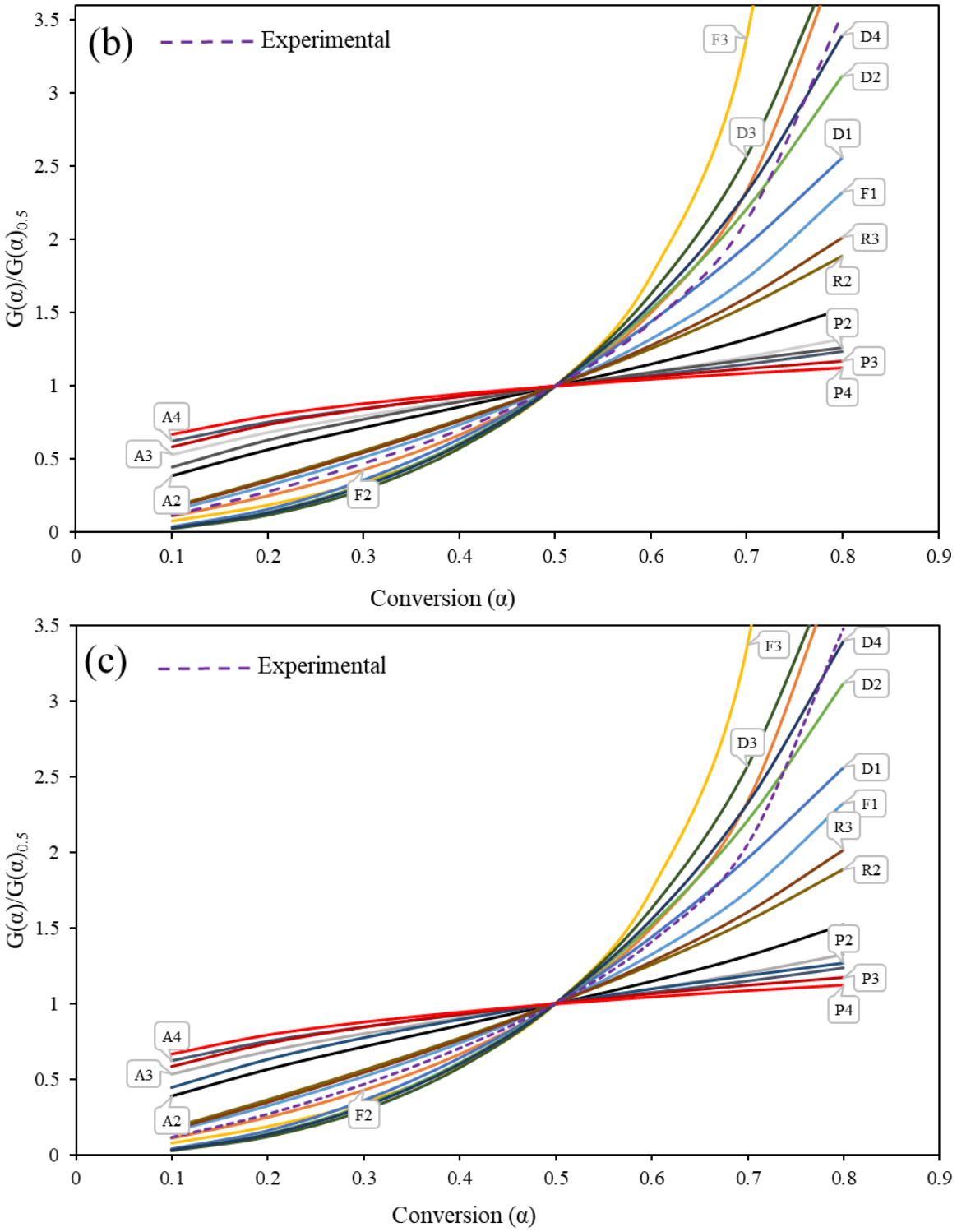

Figure 4. Comparison between theoretical master plots generated from kinetic models in Table 1 and the generalized master plots generated from experimental curves (a) for SD, (b) SD-LS and (C) SD-NZ, recorded under heating rate 40 °C min^{-1}.

The pre-exponential factor (A) and other thermal decomposition parameters such as activation enthalpy (ΔH), activation entropy (ΔS) and activation Gibbs energy (ΔG) were calculated and the results are presented in **Table 5**. The mean value of A obtained were 6.9 $\times 10^{13}$, 7.88 $\times 10^{13}$ and 8.87 $\times 10^{13}$ for SD at heating rates 35, 40 and 45 °C respectively. For SD-LS the mean A values obtained at heating rates 35, 40 and 45 °C were 1.40 $\times 10^{10}$, 1.56 $\times 10^{10}$, and 1.75$\times 10^{10}$ respectively. For SD-NZ the mean A values obtained at heating rates 35, 40 and 45 °C were 6.9 $\times 10^{10}$, 7.89 $\times 10^{10}$, and 8.87$\times 10^{10}$ s^{-1} respectively. The A values $\geq 10^9$ s^{-1} indicate a complex reaction, while the values $\leq 10^9$ s^{-1} indicate a surface reaction.[32] The values of A in between 10^{10} and 10^{12} s^{-1} indicate that the activated complex was restricted in rotation when compared to initial reagent.[41] The values of A varied with conversion but with a very narrow range, indicating the reliability of the E_α values. The activation enthalpy can be defined as the amount of energy exchanged during a chemical reaction. From Table 5 it can be observed that the changes in the activation enthalpies explaining the energy difference between the activated complex and reagent agreed with the activation energies. When the E_α values are compared against the ΔH values for all the samples considered for pyrolysis, a small energy barrier (~5 kJ mol^{-1}) indicate the possibility of the reaction happening under chosen conditions, as the literature point out that the lower difference in E_α and ΔH indicate the favorable conditions for the formation of activated complex.[40] As the enthalpy is the amount of energy utilized all through the thermal conversion of biomass material into resultant products, the closeness of ΔH and E_α indicates the additional energy required to achieve the product formation, in this case, ~ 5 kJ mol^{-1}. The activation entropy (ΔS) is associated with the formation of complex activated species and is a measure of disorder. The low activation entropy indicates that the material has reached a state near its chemical equilibrium after undergoing some kind of physical or chemical aging process. On the

other side, high activation entropy indicates that the material is far from its own thermodynamic equilibrium. In the former case, the reactivity of the material is low and demands more time to form the activated complexes, while in the latter case, the material is highly reactive and produce activated complex in shorter retention times.[42] The positive and negative values of activation entropy can reflect the degree of arrangement of carbon layers in biomass samples.[41] All the values for ΔS reported in Table 5 were negative for SD mixed with alkali metals, which illustrated that the activated complexes formed where more organized structure when compared to initial material. The change in Gibbs free energy indicates the increase in the total energy of the system during the formation of activated complex.[33] It can be noticed from Table 5 that the change in Gibbs free energy was lower for samples mixed with alkali metals, indicating the effect of catalysts on the pyrolysis process.

Table 5. Kinetic and thermodynamic parameters of thermal degradation of SD, SD-LS and SD-NZ under the heating rate (β) of 35, 40 and 45 °C min^{-1} for conversions (α) in the 0.1-0.8 range.

Sample		E_α (kJ mol^{-1})	Pre-exponential factor, A (min^{-1}) β, (°C min^{-1})			Enthalpy, °Δ*H* (kJ mol^{-1}) β, (°C min^{-1})			Gibbs free energy, °Δ*G* (kJ mol^{-1}) β, (°C min^{-1})			Entropy, °Δ*S* (J mol^{-1}) β, (°C min^{-1})		
	α		35	40	45	35	40	45	35	40	45	35	40	45
SD	0.1	156.7	3.6×10^{12}	4.1×10^{12}	4.6×10^{12}	151.9	151.8	151.8	164.0	163.3	162.6	-18.4	-17.3	-16.4
	0.2	172.6	7.2×10^{13}	8.3×10^{13}	9.3×10^{13}	167.6	167.6	167.6	163.5	162.7	162.1	6.2	7.3	8.3
	0.3	180.5	3.2×10^{14}	3.6×10^{14}	4.1×10^{14}	175.3	175.3	175.3	163.2	162.5	161.9	18.3	19.4	20.3
	0.4	172.5	7.1×10^{13}	8.1×10^{13}	9.1×10^{13}	167.3	167.3	167.2	163.5	162.8	162.1	5.7	6.8	7.8
	0.5	172.5	7.1×10^{13}	8.1×10^{13}	9.1×10^{13}	167.1	167.1	167.1	163.5	162.8	162.1	5.5	6.6	7.6
	0.6	162.2	1.0×10^{13}	1.2×10^{13}	1.3×10^{13}	156.8	156.7	156.7	163.8	163.1	162.4	-10.7	-9.6	-8.7
	0.7	152.5	1.7×10^{12}	1.9×10^{12}	2.1×10^{12}	147.0	147.0	147.0	164.2	163.4	162.8	-25.9	-24.9	-23.9
	0.8	158.5	5.1×10^{12}	5.9×10^{12}	6.6×10^{12}	153.0	152.9	152.9	164.0	163.2	162.6	-16.6	-15.5	-14.6
SD-LS	0.1	95.1	6.9×10^{7}	7.8×10^{7}	8.8×10^{7}	90.4	90.3	90.3	159.3	158.6	158.0	-108.7	-107.7	-106.7
	0.2	108.6	1.0×10^{9}	1.1×10^{9}	1.3×10^{9}	103.6	103.6	103.6	158.6	157.9	157.3	-86.7	-85.6	-84.7
	0.3	118.4	7.1×10^{9}	8.1×10^{9}	9.1×10^{9}	113.4	113.3	113.3	158.1	157.4	156.8	-70.6	-69.5	-68.6
	0.4	119.1	8.0×10^{9}	9.2×10^{9}	1.0×10^{10}	113.9	113.9	113.9	158.1	157.4	156.8	-69.7	-68.6	-67.7
	0.5	118.4	7.1×10^{9}	8.1×10^{9}	9.0×10^{9}	113.2	113.2	113.1	158.1	157.4	156.8	-70.9	-69.8	-68.9

	0.6	121.7	1.3×10^{10}	1.5×10^{10}	1.7×10^{10}	116.4	116.3	116.3	158.0	157.3	156.7	-65.6	-64.6	-63.6
	0.7	127.7	4.4×10^{10}	5.0×10^{10}	5.6×10^{10}	122.3	122.2	122.2	157.7	157.0	156.4	-55.9	-54.9	-53.9
	0.8	125.4	2.8×10^{10}	3.2×10^{10}	3.6×10^{10}	119.9	119.9	119.9	157.8	157.1	156.5	-59.8	-58.7	-57.8
SD-NZ	0.1	113.08	2.8×10^{9}	3.2×10^{9}	3.6×10^{9}	108.3	108.2	108.2	157.3	156.6	156.0	-77.3	-76.2	-75.3
	0.2	114.62	3.9×10^{9}	4.4×10^{9}	5.0×10^{9}	109.6	109.6	109.6	157.2	156.5	155.9	-75.0	-73.9	-73.0
	0.3	109.54	1.4×10^{9}	1.6×10^{9}	1.8×10^{9}	104.5	104.4	104.4	157.5	156.8	156.1	-83.6	-82.5	-81.6
	0.4	108.57	1.2×10^{9}	1.3×10^{9}	1.5×10^{9}	103.4	103.4	103.3	157.5	156.8	156.2	-85.3	-84.3	-83.3
	0.5	111.02	1.9×10^{9}	2.1×10^{9}	2.4×10^{9}	105.8	105.7	105.7	157.4	156.7	156.1	-81.4	-80.3	-79.4
	0.6	122.02	1.7×10^{10}	1.9×10^{10}	2.2×10^{10}	116.7	116.7	116.6	156.9	156.2	155.6	-63.4	-62.3	-61.4
	0.7	120.41	1.2×10^{10}	1.4×10^{10}	1.6×10^{10}	115.0	115.0	114.9	157.0	156.3	155.6	-66.2	-65.1	-64.2
	0.8	139.2	5.1×10^{11}	5.8×10^{11}	6.6×10^{11}	133.6	133.6	133.6	156.2	155.5	154.9	-35.6	-34.5	-33.6

The validation of a given kinetic triplet may be done by plotting and comparing the curve of conversion (α) vs temperature (T) obtained from its model simulation with that derived from the experimental results. A numerical procedure was used here to build up simulated α vs. T curve in Excel and is described as follows. A column of temperatures (in °K) was set up with an incremental step dT (≤ 5 °K). Corresponding guesstimates of α were then set up for each T, here a single 'guesstimate' α of 1×10^{-9} was chosen for all values of T. The column $d\alpha/dT$ was then built (LHS of Eqn (6)), and another with $(A/\beta)\exp(-E_{\alpha}/(RT))\times f(\alpha)$, i.e. RHS of Eqn. (6). A final column with $10^{8}\times|LHS-RHS|$ was set up, ensuring non zero initial values of LHS-RHS even at low α. Finally, a macro ran the function goal seek in a loop over all the data rows for each T to achieve convergence of $(10^{8}\times|LHS-RHS|)$ towards zero by adjusting the value of α.

Fig. 5 depicts the simulated and experimental α vs T curves obtained for SD, SD-LS and SD-NZ. Overall the simulated curves were in good agreement with the experimental results, which infers that the identified kinetic parameters were accurate. Matching between simulated and experimental values was very good in the low to mid conversion range, where the conversion rate better conformed to conditions of kinetic control, and in particular the modelled α vs T curve for SD-LS at 35 °K min^{-1} superimposed the experimental curve for all conversions below 0.8. Greatest discrepancies were found for the SD 35 °K min^{-1} data, where the conversion error remained at worse below 0.1, and the temperature error was maximum below 10 °K for a given conversion. With the validation step carried out, the aim of generating meaningful modelling tools for the future design of conversion plants featuring the devolatilisation of saw dust and saw dust - catalyst mixtures was achieved.

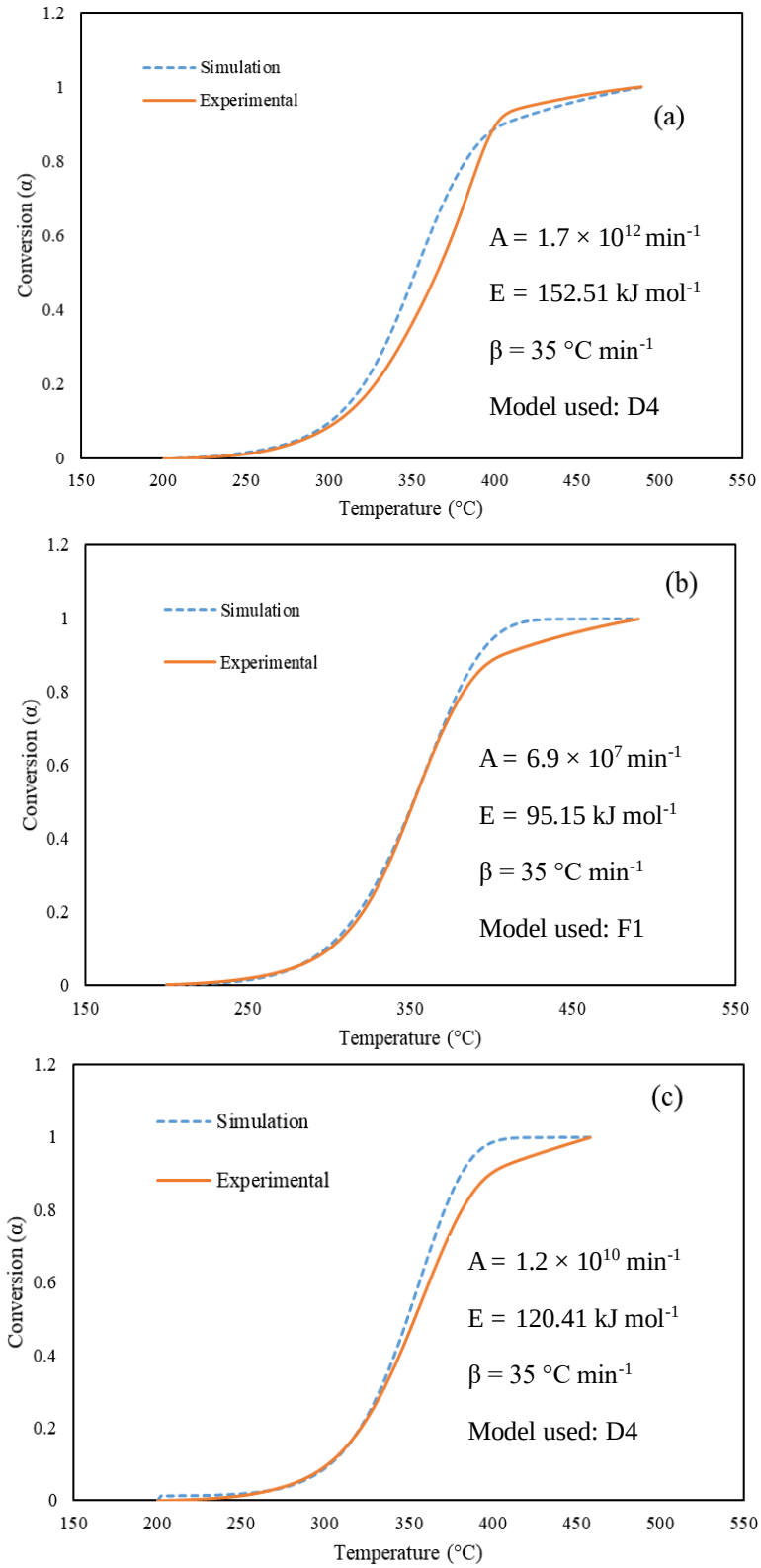

Figure 5. Simulation of (a) SD, (b) SD-LS and (c) SD-NZ pyrolysis using kinetic data obtained from FWO method and reaction mechanism obtained from master plots.

■ Conclusions

The thermal behavior of sawdust during the catalytic and non-catalytic pyrolysis was quantitatively evaluated. The presence of alkali metals leads to an early appearance of major peak of mass loss, signifying that the alkali metals appeared to catalyze reaction in the temperature range 400 – 550 °C. Furthermore, the alkali metals were effective in lowering the activation energy of sawdust pyrolysis. If heat flow and disorder change are comprehensively evaluated, the higher activation ΔG values indicated favorability for the reaction to happen. Results also showed that presence of Na_2ZrO_3 and Li_4SiO_4 increased H_2 yield during pyrolysis. Alkali metals were able to capture CO_2 released during pyrolysis and removal of CO_2 pushed the equilibrium of WGS reaction towards H_2 production.

■ AUTHOR INFORMATION

Corresponding Author

*Email: ming.zhao@tsinghua.edu.cn (Ming Zhao)

■ Author Contributions

Arun K. Vuppaladadiyam, Guozhao Ji and Ming Zhao conceived the idea and designed the experiments; Arun K. Vuppaladadiyam performed the experiments and developed the simulation model along with Valerie Dupont; Muhammad Zaki Memon and Abdul Raheem performed the data analysis and proof reading; Arun K. Vuppaladadiyam wrote the paper.

Funding Sources

The work was supported by Tsinghua University Initiative Scientific Research Program (grant number: 20161080094). EPSRC grant EP/G01244X/1 (Supergen Consortium XIV Sustainable Delivery of Hydrogen).

Notes

Any additional relevant notes should be placed here.

■ ACKNOWLEDGMENT

The work was supported by Tsinghua University Initiative Scientific Research Program (grant number: 20161080094

REFERENCES

1. Li, Z.; Liu, C.; Chen, Z.; Qian, J.; Zhao, W.; Zhu, Q., Analysis of coals and biomass pyrolysis using the distributed activation energy model. *Bioresource Technology* **2009,** 100, (2), 948-952.
2. Chen, Z.; Hu, M.; Zhu, X.; Guo, D.; Liu, S.; Hu, Z.; Xiao, B.; Wang, J.; Laghari, M., Characteristics and kinetic study on pyrolysis of five lignocellulosic biomass via thermogravimetric analysis. *Bioresource technology* **2015,** 192, 441-450.
3. Xue, S.; Lewandowski, I.; Wang, X.; Yi, Z., Assessment of the production potentials of Miscanthus on marginal land in China. *Renewable and Sustainable Energy Reviews* **2016,** 54, (Supplement C), 932-943.
4. Slopiecka, K.; Bartocci, P.; Fantozzi, F., Thermogravimetric analysis and kinetic study of poplar wood pyrolysis. *Applied Energy* **2012,** 97, (Supplement C), 491-497.
5. Wang, S.; Dai, G.; Yang, H.; Luo, Z., Lignocellulosic biomass pyrolysis mechanism: A state-of-the-art review. *Progress in Energy and Combustion Science* **2017,** 62, 33-86.
6. Trendewicz, A.; Evans, R.; Dutta, A.; Sykes, R.; Carpenter, D.; Braun, R., Evaluating the effect of potassium on cellulose pyrolysis reaction kinetics. *Biomass and Bioenergy* **2015,** 74, 15-25.
7. Memon, M. Z.; Ji, G.; Li, J.; Zhao, M., Na2ZrO3 as an Effective Bifunctional Catalyst–Sorbent during Cellulose Pyrolysis. *Industrial & Engineering Chemistry Research* **2017,** 56, (12), 3223-3230.
8. Banks, S. W.; Nowakowski, D. J.; Bridgwater, A. V., Impact of potassium and phosphorus in biomass on the properties of fast pyrolysis bio-oil. *Energy & Fuels* **2016,** 30, (10), 8009-8018.
9. Gašparovič, L.; Koreňová, Z.; Jelemenský, Ľ., Kinetic study of wood chips decomposition by TGA. *Chemical papers* **2010,** 64, (2), 174-181.

10. Burhenne, L.; Messmer, J.; Aicher, T.; Laborie, M.-P., The effect of the biomass components lignin, cellulose and hemicellulose on TGA and fixed bed pyrolysis. *Journal of Analytical and Applied Pyrolysis* **2013,** 101, (Supplement C), 177-184.
11. Zhao, B.; Xu, X.; Li, H.; Chen, X.; Zeng, F., Kinetics evaluation and thermal decomposition characteristics of co-pyrolysis of municipal sewage sludge and hazelnut shell. *Bioresource Technology* **2018,** 247, (Supplement C), 21-29.
12. Vyazovkin, S.; Burnham, A. K.; Criado, J. M.; Pérez-Maqueda, L. A.; Popescu, C.; Sbirrazzuoli, N., ICTAC Kinetics Committee recommendations for performing kinetic computations on thermal analysis data. *Thermochimica acta* **2011,** 520, (1-2), 1-19.
13. Akahira, T.; Sunose, T., Method of determining activation deterioration constant of electrical insulating materials. *Res Rep Chiba Inst Technol (Sci Technol)* **1971,** 16, 22-31.
14. Ozawa, T., A new method of analyzing thermogravimetric data. *Bulletin of the chemical society of Japan* **1965,** 38, (11), 1881-1886.
15. Flynn, J. H.; Wall, L. A., General treatment of the thermogravimetry of polymers. *J Res Nat Bur Stand* **1966,** 70, (6), 487-523.
16. Sánchez-Jiménez, P. E.; Pérez-Maqueda, L. A.; Perejón, A.; Criado, J. M., Generalized master plots as a straightforward approach for determining the kinetic model: the case of cellulose pyrolysis. *Thermochimica acta* **2013,** 552, 54-59.
17. Poletto, M.; Zattera, A. J.; Santana, R. M. C., Thermal decomposition of wood: Kinetics and degradation mechanisms. *Bioresource Technology* **2012,** 126, 7-12.
18. Ali, I.; Naqvi, S. R.; Bahadar, A., Kinetic analysis of Botryococcus braunii pyrolysis using model-free and model fitting methods. *Fuel* **2018,** 214, 369-380.
19. Zhao, M.; Fan, H.; Yan, F.; Song, Y.; He, X.; Memon, M. Z.; Bhatia, S.; Ji, G., Kinetic analysis for cyclic CO2 capture using lithium orthosilicate sorbents derived from different silicon precursors. *Dalton Transactions* **2018**.
20. Ji, G.; Memon, M. Z.; Zhuo, H.; Zhao, M., Experimental study on CO2 capture mechanisms using Na2ZrO3 sorbents synthesized by soft chemistry method. *Chemical Engineering Journal* **2017,** 313, 646-654.
21. Mishra, G.; Bhaskar, T., Non isothermal model free kinetics for pyrolysis of rice straw. *Bioresource technology* **2014,** 169, 614-621.
22. Friedman, H. L., Kinetics of thermal degradation of char-forming plastics from thermogravimetry. Application to a phenolic plastic. *Journal of Polymer Science Part C: Polymer Symposia* **1964,** 6, (1), 183-195.
23. Gotor, F. J.; Criado, J. M.; Malek, J.; Koga, N., Kinetic analysis of solid-state reactions: the universality of master plots for analyzing isothermal and nonisothermal experiments. *The journal of physical chemistry A* **2000,** 104, (46), 10777-10782.
24. Vyazovkin, S., Kinetic concepts of thermally stimulated reactions in solids: A view from a historical perspective. *International Reviews in Physical Chemistry* **2000,** 19, (1), 45-60.
25. Zubair, M.; Shehzad, F.; Al-Harthi, M. A., Impact of modified graphene and microwave irradiation on thermal stability and degradation mechanism of poly (styrene-co-methyl meth acrylate). *Thermochimica Acta* **2016,** 633, 48-55.
26. Senum, G.; Yang, R., Rational approximations of the integral of the Arrhenius function. *Journal of thermal analysis* **1977,** 11, (3), 445-447.
27. Huang, L.; Xie, C.; Liu, J.; Zhang, X.; Chang, K.; Kuo, J.; Sun, J.; Xie, W.; Zheng, L.; Sun, S., Influence of catalysts on co-combustion of sewage sludge and water hyacinth blends as determined by TG-MS analysis. *Bioresource technology* **2018,** 247, 217-225.

28. Kim, Y. S.; Kim, Y. S.; Kim, S. H., Investigation of Thermodynamic Parameters in the Thermal Decomposition of Plastic Waste−Waste Lube Oil Compounds. *Environmental Science & Technology* **2010,** 44, (13), 5313-5317.
29. Zhang, G.; Sun, Y.; Shi, Y.; Jia, Y.; Xu, Y.; Zhao, P.; Zhang, Y., Characteristic and kinetics of corn stalk pyrolysis in a high pressure reactor and steam gasification of its char. *Journal of analytical and applied pyrolysis* **2016,** 122, 249-257.
30. Zhao, B.; Xu, X.; Li, H.; Chen, X.; Zeng, F., Kinetics evaluation and thermal decomposition characteristics of co-pyrolysis of municipal sewage sludge and hazelnut shell. *Bioresource technology* **2018,** 247, 21-29.
31. Cai, J.; Xu, D.; Dong, Z.; Yu, X.; Yang, Y.; Banks, S. W.; Bridgwater, A. V., Processing thermogravimetric analysis data for isoconversional kinetic analysis of lignocellulosic biomass pyrolysis: Case study of corn stalk. *Renewable and Sustainable Energy Reviews* **2018,** 82, 2705-2715.
32. Turmanova, S. C.; Genieva, S.; Dimitrova, A.; Vlaev, L., Non-isothermal degradation kinetics of filled with rise husk ash polypropene composites. *Express Polymer Letters* **2008,** 2, (2), 133-146.
33. Maia, A. A. D.; de Morais, L. C., Kinetic parameters of red pepper waste as biomass to solid biofuel. *Bioresource Technology* **2016,** 204, 157-163.
34. Gai, C.; Dong, Y.; Zhang, T., The kinetic analysis of the pyrolysis of agricultural residue under non-isothermal conditions. *Bioresource Technology* **2013,** 127, 298-305.
35. Garcia-Maraver, A.; Perez-Jimenez, J. A.; Serrano-Bernardo, F.; Zamorano, M., Determination and comparison of combustion kinetics parameters of agricultural biomass from olive trees. *Renewable Energy* **2015,** 83, 897-904.
36. Zhu, F.; Feng, Q.; Xu, Y.; Liu, R.; Li, K., Kinetics of pyrolysis of ramie fabric wastes from thermogravimetric data. *Journal of Thermal Analysis and Calorimetry* **2015,** 119, (1), 651-657.
37. Yang, H.; Yan, R.; Chen, H.; Lee, D. H.; Zheng, C., Characteristics of hemicellulose, cellulose and lignin pyrolysis. *Fuel* **2007,** 86, (12-13), 1781-1788.
38. Braga, R. M.; Melo, D. M. A.; Aquino, F. M.; Freitas, J. C. O.; Melo, M. A. F.; Barros, J. M. F.; Fontes, M. S. B., Characterization and comparative study of pyrolysis kinetics of the rice husk and the elephant grass. *Journal of Thermal Analysis and Calorimetry* **2014,** 115, (2), 1915-1920.
39. Li, D.; Chen, L.; Zhang, X.; Ye, N.; Xing, F., Pyrolytic characteristics and kinetic studies of three kinds of red algae. *Biomass and Bioenergy* **2011,** 35, (5), 1765-1772.
40. Mehmood, M. A.; Ye, G.; Luo, H.; Liu, C.; Malik, S.; Afzal, I.; Xu, J.; Ahmad, M. S., Pyrolysis and kinetic analyses of Camel grass (Cymbopogon schoenanthus) for bioenergy. *Bioresource Technology* **2017,** 228, 18-24.
41. Xu, Y.; Chen, B., Investigation of thermodynamic parameters in the pyrolysis conversion of biomass and manure to biochars using thermogravimetric analysis. *Bioresource Technology* **2013,** 146, 485-493.
42. Ruvolo-Filho, A.; Curti, P. S., Chemical kinetic model and thermodynamic compensation effect of alkaline hydrolysis of waste poly (ethylene terephthalate) in nonaqueous ethylene glycol solution. *Industrial & engineering chemistry research* **2006,** 45, (24), 7985-7996.